

Multi-cracking modelling in concrete solved by a modified DR method

Rena C. Yu[†] and Gonzalo Ruiz[‡]

*ETSI de Caminos, C. y P., Universidad de Castilla-La Mancha
Avda. Camilo José Cela, s/n, 13071 Ciudad Real, Spain
(Received May 19, 2004, Accepted September 13, 2004)*

Abstract. Our objective is to model static multi-cracking processes in concrete. The explicit dynamic relaxation (DR) method, which gives the solutions of non-linear static problems on the basis of the steady-state conditions of a critically damped explicit transient solution, is chosen to deal with the high geometric and material non-linearities stemming from such a complex fracture problem. One of the common difficulties of the DR method is its slow convergence rate when non-monotonic spectral response is involved. A modified concept that is distinct from the standard DR method is introduced to tackle this problem. The methodology is validated against the stable three point bending test on notched concrete beams of different sizes. The simulations accurately predict the experimental load-displacement curves. The size effect is caught naturally as a result of the calculation. Micro-cracking and non-uniform crack propagation across the fracture surface also come out directly from the 3D simulations.

Keywords: dynamic relaxation; cohesive element; self adaptive remeshing.

1. Introduction

Our objective is to model static multi-cracking processes in quasi-brittle materials like concrete. The viability of cohesive theories of fracture applied to the dynamic regime has been demonstrated and documented by Ortiz and his coworkers (Camacho and Ortiz 1996, Ortiz and Pandolfi 1999, Pandolfi, *et al.* 1999, Ruiz, *et al.* 2000, 2001, Yu, *et al.* 2002, 2004). Multi-cracking processes were modeled by inserting cohesive surfaces between the elements defining the original mesh. The crack propagation was led by a fragmentation algorithm that was able to modify the topology of the mesh at each loading step (Ortiz and Pandolfi 1999, Pandolfi and Ortiz 1998, 2002). However, the modeling of crack propagation within static regime has been hindered by the difficulty of finding efficient and stable numerical algorithms which are able to deal with high geometric and material non-linearities.

One feasible way to solve non-linear static problems is based on the steady-state conditions of a critically damped transient solution, often termed as dynamic relaxation (DR). Searching for the solution, the DR method sets an artificial dynamic system of equations with added fictitious inertia and damping terms, and lets it *relax* itself to the real solution of the physical problem. Since Day (1965) first introduced the method in the 1960s, this simple and effective way of dealing with non-

[†] Researcher Ramon y Cajal

[‡] Associate Professor

linear problems has been used for some decades in general structural applications (Day 1965, Otter 1965, Brew and Brotton 1971, Pica and Hinton 1980, Papadrakakis 1981, Underwood, 1983, Sauvé and Metzger 1995), in rolling (Chen, *et al.* 1989), bending with wrinkling (Zhang and Yu 1989) as well as creep (Sauvé and Badie 1993). Siddiquee (1995) also used DR to trace the equilibrium path in materially non-linear problems. Essentially, the DR method is used to maintain the advantages of an explicit methodology compared to an otherwise implicit approach. In principle, if the physical problem has a solution, this solution can be reached *sooner or later*, at which point the challenge becomes efficiently enhancing the relaxation process.

Besides the use of parallel computing, different aspects of the effectiveness of DR have been investigated by a series of authors, for instance, adaptively adjusting the loading rate by Rericha (1986), adaptive damping in kinematically loaded situations by Sauvé (1996) or the effect of constraints and mesh transitions on convergence rate by Metzger (1997). Over the years, a general procedure for DR has been formulated to solve a wide range of problems, this includes a lumped mass matrix, a mass proportional damping matrix and a standard procedure to estimate the damping coefficient based on the participating frequency of the structural response (Rayleigh's quotient). Consequently, Oakley and Knight (1995a, 1995b, 1995c, 1996) have given detailed implementations for single processors as well as parallel processor computers. However, the performance of DR is highly dependent on the properties of the problem (Metzger 2003).

In particular, our model to study complex fracture processes in concrete is very non-linear. This nonlinearity stems both from the cohesive laws governing the opening of the cracks and from the constant insertion of new elements. The standard estimation of the critical damping coefficient through Rayleigh's quotient damps the system from higher frequency modes to lower frequency modes. When there is cracking, the estimation may give a higher frequency mode, which actually stalls the motion and makes the convergence rate unacceptably slow. For that particular situation, we have found that by damping the system in two successive steps through two criteria, the calculations can be greatly enhanced. During the first step, the system is artificially set in motion, and this motion is kept as *strong* as possible in order to be felt by the whole system; this can only be realized through *under-damping*, i.e., adopting a damping coefficient smaller than the one given by Rayleigh's quotient. Once the motion has reached the whole system, in the second step, critical damping is adopted so that the system can reach its steady state at the fastest possible rate. By doing so, the speed to achieve the convergence of the solution can be increased by a magnitude of ten or more and therefore the solution procedure becomes acceptable to the scale of the problem that we are considering here.

By underdamping the system we speed up the convergence process but, at the same time, we increase the risk of fostering cohesive crack growth to a spurious and undesirable extent. This risk is reduced here by taking the following precautions. Every load step is performed in two distinct phases. The first one searches for stability without updating the internal variables of the irreversible elements nor letting the fragmentation algorithm work. Insertion of new crack surfaces is only allowed when stability is achieved, although their presence unbalances the system again and makes a second series of iterations to regain equilibrium necessary. Only at the end of the whole step do we update the internal variables of the irreversible elements. Finally, as might be expected, the load or displacement increments are taken small compared to the scale of the problem in order to avoid considerable fragmentation and subsequent fracture activity at each particular step.

This paper is structured as follows. In the following section we briefly review the cohesive model. In Section 3 the formulation procedure of the standard explicit dynamic relaxation method is

explained. The modifications of the method proposed herein are presented in Section 4. The modified method is validated by simulating some fracture experiments on concrete specimens (Section 5): on the one hand, we compare the performance of both the standard and the modified method and check that they provide the same results (5.1); on the other hand, we validate the model against the experimental results (5.2). Finally, in Section 6 we draw some conclusions.

2. The cohesive model

As follows we summarize the main features of the cohesive model used in the calculations. A complete account of the theory and its finite-element implementation may be found elsewhere (Camacho and Ortiz 1996, Ortiz and Pandolfi 1999). A variety of mixed-mode cohesive laws accounting for tension-shear coupling (Camacho and Ortiz 1996, Ortiz and Pandolfi 1999, De Andrés, *et al.* 1999), are obtained by the introduction of an effective opening displacement δ , which assigns different weights to the normal δ_n and sliding δ_s opening displacements,

$$\delta = \sqrt{\beta^2 \delta_s^2 + \delta_n^2} \quad (1)$$

Assuming that the cohesive free-energy density depends on the opening displacements only through the effective opening displacement δ , a reduced cohesive law, which relates δ to an effective cohesive traction

$$t = \sqrt{\beta^2 t_s^2 + t_n^2} \quad (2)$$

where t_s and t_n are the shear and the normal tractions respectively, can be obtained (Camacho and Ortiz 1996, Ortiz and Pandolfi 1999). The weighting coefficient β defines the ratio between the shear and the normal critical tractions. It is considered a material parameter that measures the ratio of the shear and tensile resistance of the material. The existence of a loading envelope defining a connection between t and δ under the conditions of monotonic loading, and irreversible unloading is assumed. A simple and convenient type of irreversible cohesive law, typically used for concrete for it is recommended by the Model Code (1993), is furnished by following the bi-linearly decreasing envelope

$$t = \begin{cases} f_{ts}(1 - 0.85\delta/\delta_A) & 0 \leq \delta \leq \delta_A \\ 0.15f_{ts}(\delta_c - \delta)/(\delta_c - \delta_A) & \delta_A \leq \delta \leq \delta_c \\ 0 & \delta \geq \delta_c \end{cases} \quad (3)$$

where f_{ts} is the tensile strength, δ_c is the critical opening displacement and δ_A , and δ_c are determined through the following equations

$$\delta_A = (2 - 0.15\beta_F)G_c/f_{ts}$$

$$\delta_c = \beta_F G_c/f_{ts}$$

in which G_c is the material fracture energy and β_F is related to the maximum aggregate size d_m

through the expression

$$\beta_F = 9 - \frac{1}{8}d_m$$

Cohesive theories introduce a well-defined length scale into the material description and, in consequence, are sensitive to the size of the specimen (see, for example, Bazant and Planas 1998). The characteristic length of the material may be expressed as

$$l_c = \frac{EG_c}{f_{ts}^2} \quad (4)$$

where E is the material elastic modulus.

In the calculation, only decohesion along element boundaries is allowed to occur. When the critical cohesive traction is attained at the interface between two volume elements, a cohesive element is inserted at that location using a fragmentation algorithm (Pandolfi and Ortiz 2002). The cohesive element subsequently governs the opening of the cohesive surface.

3. The explicit dynamic relaxation method

As mentioned earlier, in calculations, the fracture surface is confined to inter-element boundaries and, consequently, the structural cracks predicted by the analysis are necessarily rough. Even though this numerical roughness in concrete can be made to correspond to the physical roughness by simply choosing the element size to resolve the cohesive zone size (Ruiz, *et al.* 2001), the non-linearity of the solution thus induced plus the material non-linearity is difficult to handle in static regime for traditional solvers. We choose the explicit dynamic relaxation method as an alternative to tackle this situation, the standard formulation of this methodology is summarized below.

Consider the system equations for a static problem at a certain load step n :

$$F^{int}(u_n) = F_n^{ext} \quad (5)$$

where u_n is the solution array (displacements), F^{int} and F_n^{ext} are the internal and the external force vectors. Following the ideas of dynamic relaxation, Eq. (5) is transformed into a dynamic system by adding both artificial inertia and damping terms.

$$M\ddot{u}_n + C\dot{u}_n + F^{int}(u_n) = F_n^{ext} \quad (6)$$

where M and C are the fictitious mass and damping matrices, \ddot{u}_n and \dot{u}_n are the acceleration and the velocity arrays respectively at load step n . The solution of Eq. (6) can be obtained by the explicit time integration method using the standard central difference integration scheme in two steps.

First the displacements and predictor velocities are obtained:

$$u_n^{t+1} = u_n^t + \Delta t \dot{u}_n^t + \frac{1}{2} \Delta t^2 \ddot{u}_n^t \quad (7)$$

$$\dot{u}_{npred}^{t+1} = \dot{u}_n^t + \frac{1}{2} \Delta t \ddot{u}_n^t \quad (8)$$

Then we update the internal force vector and obtain the accelerations and corrected velocities:

$$\ddot{u}_n^{t+1} = \left(M + \frac{1}{2} \Delta t C \right)^{-1} [F_n^{ext} - F_n^{int}(u_n^{t+1}) - C \dot{u}_{pred}^{t+1}] \quad (9)$$

$$\dot{u}_n^{t+1} = \dot{u}_{npred}^{t+1} + \frac{1}{2} \Delta t \ddot{u}_n^{t+1} \quad (10)$$

Please notice that Eqs. (7) through (10) are obtained from the explicit Newmark scheme, which dictates C to be diagonal. Additionally, as pointed out by Cook, *et al.* (1989), the presence of damping in the explicit Newmark scheme *raises* the stability limit, which is in contrast to other forms of the central-difference method in which no change, or a decrease in the stability limit, are observed.

It is customary to eliminate C through the following equation

$$C = \xi M \quad (11)$$

where ξ is the damping ratio, and to set both fictitious mass M and damping C matrices to be diagonal to preserve the explicit form of the time-stepping integrator.

To ensure that the mode associated with the applied loading condition is critically damped, ξ is generally set to be

$$\xi = 2\omega \quad (12)$$

where ω is the undamped natural frequency corresponding to the participating mode of loading.

Since both the inertia and damping terms are artificial, the dynamic relaxation parameters, including the mass matrix M , the damping coefficient ξ and the time step Δt , can be selected to produce faster and more stable convergence to the static solution of the real physical system.

Owing to the explicit formulation the time step can be conservatively estimated from the undamped system. It must satisfy the stability condition

$$\Delta t \leq h_{\min} / c_d \quad (13)$$

where h_{\min} is the size of the smallest element and c_d is the dilatational wave speed, which in turn, can be related to ω_{\max} , the highest undamped frequency of the discretized system

$$\omega_{\max} = 2c_d / h_{\min} \quad (14)$$

For an elastic material, the dilatational wave speed is calculated as

$$c_d = \sqrt{(\lambda + 2G) / \rho} \quad (15)$$

where λ and G are the Lamé constants, while ρ is the material density. Eqs. (13), (14) and (15) provide a correlation between the maximum admissible time step, $\Delta t_{cr} = 2 / \omega_{\max}$, and the fictitious mass matrix:

$$\rho \geq (\lambda + 2G) \left(\frac{\Delta t_{cr}}{h} \right)^2 \quad (16)$$

In this implementation, the density is adjusted for each element so that the time for the elastic wave to travel through every element is the same. The diagonal mass matrix is obtained through the nodal lumping scheme used in the composite element defined by Thoutireddy, *et al.* (2002) where four vertex have the weight 1/32 and the mid-side nodes have the weight 7/48.

Underwood (1983) pointed out that the convergence rate of dynamic relaxation is given in terms of the spectral radius of the iterative error equations

$$R_{spr} \approx \left| 1 - 2 \frac{\omega}{\omega_{\max}} \right| \quad (17)$$

where ω and ω_{\max} are the lowest and highest frequencies of the discretized equations of motion. By maximizing the ratio ω/ω_{\max} , and therefore minimizing the spectral radius, a faster convergence rate can be obtained. As observed by Underwood (1983), the way of estimating the fictitious mass matrix that has been described above produces a scaling in the frequencies that generally increases the ratio ω/ω_{\max} for faster convergence and that at the very least, does not reduce it.

In these calculations, the time increment acts as an iteration counter. So, if we set it to be 1, the highest frequency ω_{\max} has a fixed value of 2, whereas ω is based on the lowest participating mode of the structure corresponding to the load distribution. In this work, the procedure to estimate the critical damping coefficient suggested by Underwood (1983) and Oakley (1995b) is implemented. The current value of ω is estimated at each iteration t using Rayleigh's quotient

$$\omega^t = \sqrt{\frac{(x^t)^T K^t x^t}{(x^t)^T M x^t}} \quad (18)$$

where x^t stands for the eigenvector associated with ω^t at the t^{th} iteration. For non-linear problems, K represents a diagonal estimate of the tangent stiffness matrix at the t^{th} iteration, which is given by

$$K^t = \frac{F^{int}(u_n^t) - F^{int}(u_n^{t-1})}{u_n^t - u_n^{t-1}}. \quad (19)$$

The displacement increment vector, which better represents the local deformation mode, is utilized for the vector x^t in Eq (18). This choice also allows us to get the simpler expression of ω^t in Eq. (22), Table 1, which eliminates the possibility of zeros in the denominator.

4. The modified DR method

As we mentioned earlier, one of the common difficulties of the DR method is its slow convergence rate when non-monotonic spectral response is involved. The standard estimation of the critical damping coefficient is done through Rayleigh's quotient, which damps the system from higher frequency modes to lower frequency modes. During the calculations for non-linear problems, when the estimation gives a higher frequency mode, the damping coefficient adopted will overdamp the global motion and actually stall the system, making the convergence rate unacceptably slow. In dealing with this difficulty, instead of critically damping the system equations from the beginning as suggested by all the standard DR procedures, we intend to keep the motion as *strong* as possible, so that the local movement provoked at the loading area or at the crack tip can spread to the rest. This

can only be done through *under-damping*, i.e., adopting a damping coefficient smaller than the one estimated by the current Rayleigh estimation. No-damping or low damping would not work since this may lead to a persistent noisy response (Metzger 2003). We found that by setting the damping coefficient close to half of the one corresponding to the undamaged system (which was obtained through the Rayleigh quotient estimation in the trial run), the motion can be kept strong so that the system could move faster toward its external force equilibrium avoiding an incessant noisy response. Once the external force equilibrium is achieved, the system is critically damped to its steady state to obtain the static solution.

Taking into account the aforementioned considerations, we implement two combined convergence criteria to be used during the iteration process. One is the ratio between the sum of the external forces plus the reaction forces over the estimated maximum external forces, which is a measure that says to what extent the motion has spread to the whole system. The other is the relative global kinetic energy, which measures whether the system is static or not. These are characterized by the following inequalities:

$$\text{(error norm 1)} \quad \frac{\|F_r + F_i\|_2}{\|F_{ext}\|_2} < f_{tol} \quad (20)$$

$$\text{(error norm 2)} \quad \frac{\sum \frac{1}{2} m (\dot{u}')^2}{K_0} < k e_{tol} \quad (21)$$

where $\|o\|_2$ denotes the Euclidean norm, F_r is the sum of the reaction forces at the supports, F_i is the external force at the loading point, F_{ext} is the maximum value of the external force at the loading point, m is the nodal mass and K_0 is a constant used to normalize the kinetic energy. The values of F_{ext} and K_0 vary according to the scale of the problem. They can be adjusted, respectively, to the maximum external force and kinetic energy observed as the system evolves. F_{ext} and K_0 can also be chosen in accordance with experimental data on condition that such information is available.

By underdamping the system we speed up the convergence process but, at the same time, we increase the risk of overshooting the cohesive elements that are already inserted at the previous load step, for they behave irreversibly to reproduce the damage caused by the fracture process. It also could happen that the conditions for the insertion of new elements were met while the system was underdamped, which could lead to a spurious crack surface. Of course, bulk elements could also be overshoot if their constitutive equation included plasticity or any other feature to represent crushing.

In our case the problem of overshooting is reduced by taking the following precautions. Every load step is performed in two distinct phases. The first one searches for stability without updating the internal variables of the irreversible elements nor letting the fragmentation algorithm work. Insertion of new elements is only allowed when stability is achieved, although the formation of new crack surfaces unbalance the system again and make a second series of iterations to regain equilibrium necessary. Only at the end of the whole step do we update the internal variables of the cohesive elements. Finally, as might be expected, the load or displacement increments are taken small compared to the scale of the problem in order to avoid considerable fragmentation and subsequent fracture activity at each particular step.

The algorithm as implemented is summarized in Table 1, where ξ^0 is the damping coefficient computed in the program after the first insertion of the cohesive element takes place, or when the non-linearity of the material started to emerge. By setting the damping coefficient to this value

Table 1 Modified explicit dynamic relaxation algorithm

1. Get F_{int} from initial condition and initialize M for $\Delta t = 1.01$ for each element.

2. At iteration t

(i) compute displacements and predictor velocities at $t + 1$:

$$u_n^{t+1} = u_n^t + \Delta t \dot{u}_n^t + 1/2 \Delta t^2 \ddot{u}_n^t,$$

$$\dot{u}_{npred}^{t+1} = \dot{u}_n^t + 1/2 \Delta t^2 \ddot{u}_n^t;$$

(ii) compute internal forces $F^{int}(u_n^t)$ and calculate residuals

$$R_n^t = F_n^{ext} - F^{int}(u_n^t);$$

(iii.1) evaluate current damping coefficient ξ^t :

$$\Delta u_n = u_n^t - u_n^{t-1},$$

$$\omega^t = \frac{\sqrt{(\Delta u_n^t)(F_{int}^t - F_{int}^{t-1})}}{\sqrt{(\Delta u_n^t)^T M (\Delta u_n^t)}}, \quad (22)$$

$$\xi^t = 2\omega^t;$$

(iii.2) if error norm $1 > 1.1 f_{tol}$ and $\xi^t > 0.3 \xi_{max}$, set $\xi^t = \xi^0$;

(iv) compute accelerations and velocities at $t + 1$:

$$\ddot{u}_n^{t+1} = (M + 1/2 \Delta t \xi^t M)^{-1}$$

$$[F_n^{ext} - F^{int}(u_n^{t+1}) - \xi^t M \dot{u}_{npred}^t],$$

$$\dot{u}_n^{t+1} = \dot{u}_{npred}^{t+1} + 1/2 \Delta t \ddot{u}_n^{t+1};$$

(v) check error norm

$$\frac{\|F_r + F_i\|_2}{\|F_{ext}\|_2} < f_{tol},$$

$$\frac{\sum \frac{1}{2} m (\dot{u}_n^t)^2}{K_0} < k e_{tol} \quad ;$$

if satisfied, compute stress and strain vectors, update internal variables and move to the next load step $n+1$;

(vi). Otherwise, go to (i) and set $t = t + 1$.

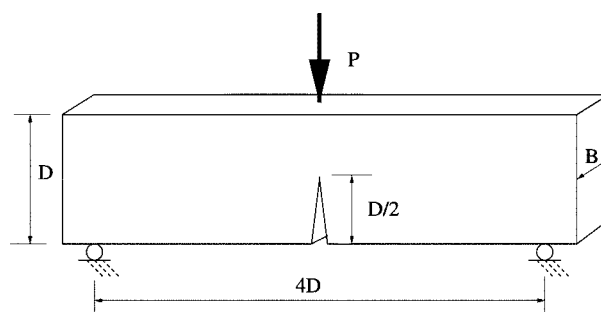


Fig. 1 A notched concrete beam subjected to three point bending

Table 2 Concrete mechanical properties

f_{ts} (MPa)	E (GPa)	ν	G_c (N/m)	l_{ch} (mm)
3.8	30.5	0.2	62.5	130

when the solution is far from equilibrium and the estimated frequency is high, the global convergence rate is remarkably enhanced. The details are going to be shown later on with the examples.

5. Numerical applications

We apply the modified dynamic relaxation method to solve the static crack propagation through a notched concrete beam subjected to three point bending, see Fig. 1. Particularly, we use the experiments in Ruiz (1999): three specimens, with depth $D = 75, 150$ and 300 mm respectively, all with the same thickness $B = 50$ mm are modeled. The material parameters for the concrete given in Table 2 are also taken from Ruiz (1999). The cohesive law adopted in the calculation is the one suggested in the Model Code (1993) for concrete, Eq. (3).

In previous studies, Camacho and Ortiz (1996) have noted that the accurate description of fracture processes by means of cohesive elements requires the resolution of the characteristic cohesive length of the material. Further studies (Ruiz, *et al.* 2001) showed that in concrete, the element size can be made to be comparable to the minimum aggregate size, which is 5 mm in our case. So all specimens are discretized into ten-node quadratic tetrahedral elements and have an element size of 6 mm near the middle surface. Figs. 2a, b and c show the mesh used in the calculations for the small, medium and large size specimens, which consists of 2103, 4048 and 10745 10-node quadratic tetrahedrons, respectively. Concrete bulk is modeled as a finite elastic Neo-Hookean material extended to the compressible range.

Regarding the tolerances defined in Eq. (21), the product $\|F_{ext}\|_2 f_{tol}$ is taken as 1 N for all the simulations, whereas the product $K_0 k_{e_{tol}}$ is taken as 10^{-8} , 10^{-7} and 5×10^{-7} Nmm for the small, intermediate and big specimens respectively.

For the purpose of having an order of magnitude in the case of the error norm 1, please remember that $\|F_{ext}\|_2$ in Eq. (21) represents the modulus of the maximum external force and thus it varies with the scale of the problem. Here we use the experimental values for $\|F_{ext}\|_2$, which were 800, 1300 and 1800 N for the 75, 150 and 300 mm deep beams respectively. Likewise, in the case of the

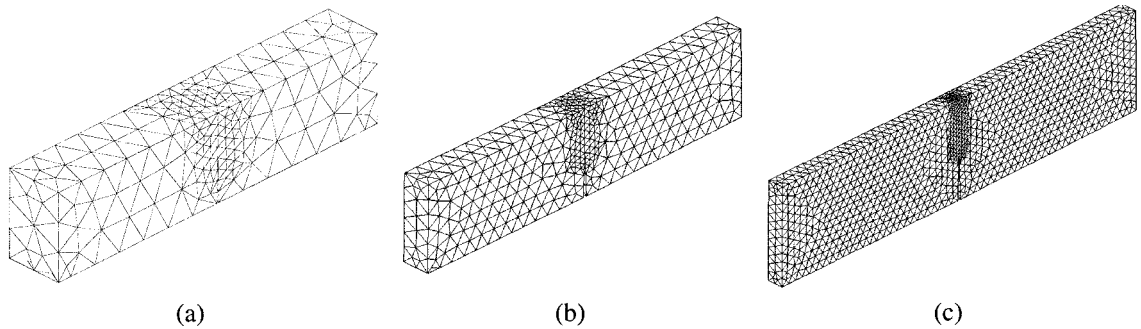


Fig. 2 The meshes used in the simulations for $D =$ (a) 75 mm; (b) 150 mm; (c) 300 mm

error norm 2, a convenient choice for K_0 in our simulations is the fracture energy expenditure for each size. This is equivalent to the work of the external forces throughout the whole fracture process and was measured in the experiments. Its value can be obtained by the product of the specific fracture energy A_3 and the fracture surface created in each size, which is $DB/2$. This multiplication gives 117, 234 and 469 Nmm, the results ordered by size. So, convergence is achieved in the small beam when the out-of-balance forces are 0.125% of the maximum external force applied on it and when the total kinetic energy is 8.5×10^{-9} % of the total energy consumed by the fracture process. The corresponding percentages for the intermediate size beam are 0.077 and 4.3×10^{-8} while for the big beam the figures are 0.055 and 1.1×10^{-7} .

Before starting to run the model, it is also necessary to set the damping coefficient defining the verge of an acceptable damping. Our choice for this particular problem, after several trial runs, is $0.3\xi_{\max}$ ($\approx 20\xi^0$ in this case), as indicated in Table 1 (command iii. 2). The trial runs showed that the behavior of the model is not very sensitive to this parameter, i.e., small variations of it lead to small changes in the convergence rate.

5.1. Comparison between the standard and the modified DR procedures

In this section, we choose one loading step within the simulation of the small specimen to show the improved convergence rate using the modified DR method. We also check that the modified method does not affect the final result in any detrimental way by comparing with the results obtained with the standard DR method. The step chosen corresponds to an imposed displacement of $d = 0.0224$ mm. In the previous step there were already four cohesive elements inserted, i.e., the step corresponds to the initiation of the crack and the system may evolve irreversibly even if there were no crack advance.

As mentioned in Section 4, when searching for the solution of a particular step, we divide the iteration process into two phases. During the first phase the specimen is loaded by a small increase of the imposed displacement and is left to evolve until equilibrium is reached. During this phase we do not activate the fragmentation algorithm nor do we update the internal variables of the elements so that no irreversible processes may take place. Actually, as the tetrahedrons are Neo-Hookean, the only possible irreversibility is concentrated on the fracture development and then, as long as there is no insertion of new elements nor any updating of the ones that are initially present, overshooting is avoided altogether. Fig. 3 shows, for both the standard and the modified method, the evolution of the out-of-balance forces and the kinetic energy of the system during the iterations belonging to this

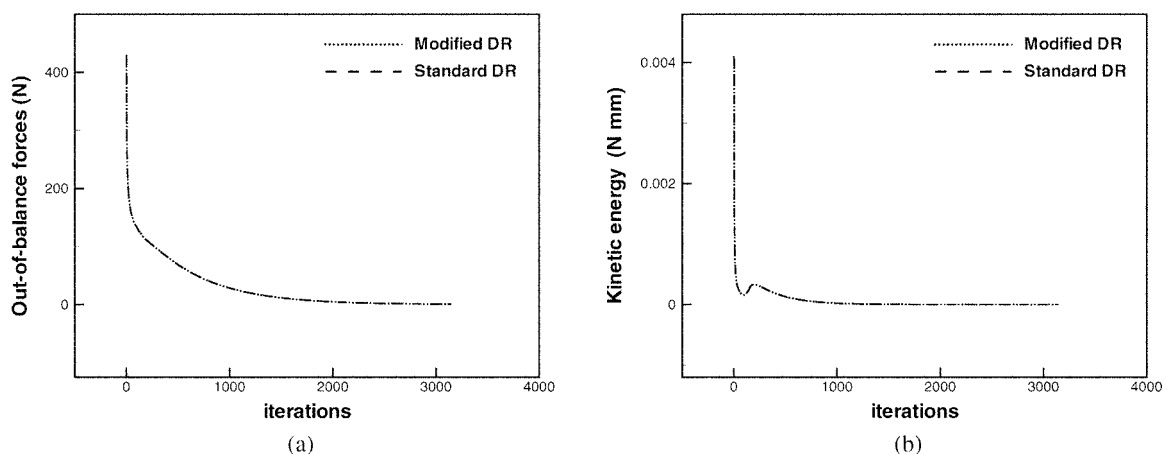


Fig. 3 Comparison between the standard and modified DR procedures: (a) Out-of-balance forces and (b) kinetic energy corresponding to the small specimen during the first phase in the step for an imposed displacement of $\delta = 0.0224$ mm

phase. In fact, the modified procedure is not activated at all during this phase because the forces are not balanced and Rayleigh's quotient gives a good estimation of the frequency of vibration of the beam.

The second phase starts when convergence has been achieved in the first one. Then the program checks the traction of all the element interfaces and, if the opening criterion is satisfied at any of them, a cohesive element is inserted there (in this particular case only two new elements are inserted). Consequently, before moving to the next displacement increment, an iteration loop is carried out to adjust the solutions because of the stress release coming from the crack propagation. The elements are updated at convergence of the second phase. Fig. 4 shows the histories of the out-of-balance forces and of the kinetic energy as the loop proceeds.

Since the dynamic equilibrium has been enhanced by previous iterations during the first phase, the two methods give the same damping forces and kinetic energy until at some point the program detects that the system is becoming unbalanced. Moreover, the frequencies generated by the insertion are considerably bigger than the ones corresponding to the imposed displacements over the undamaged beam. Thus the modified DR is activated. Fig. 4a shows that the out-of-balance forces with the modified DR method in practice are of the same order of magnitude as with the standard procedure. In this particular step they almost reach the value of 6 N (the out-of-balance forces at the beginning of the first phase were bigger than 400 N, Fig. 3a). The values of the kinetic energy at the beginning of the phase are relatively high, of the order of 0.01 Nmm according to Fig. 4b, which is almost three times the maximum energy of the first phase (Fig. 3b). By then the system is critically damped because the unbalanced forces fall under the tolerance and so the motion is rapidly stalled. When the system gets unbalanced and, consequently, underdamped, the kinetic energy starts to oscillate between 0 and 0.001 Nmm (Fig. 4c zooms the energy cycles). Please remember that the energy needed to split the specimen is 117 Nmm and thus the oscillation is five orders of magnitude below it. The movement towards the equilibrium position is relatively fast at this stage and balance is soon restored. Consequently, the damping goes back to its critical value and final convergence is achieved in a few more iterations as illustrated in Fig. 4d.

In the example shown, where the non-linearity is not strong, it takes 25785 iterations for the

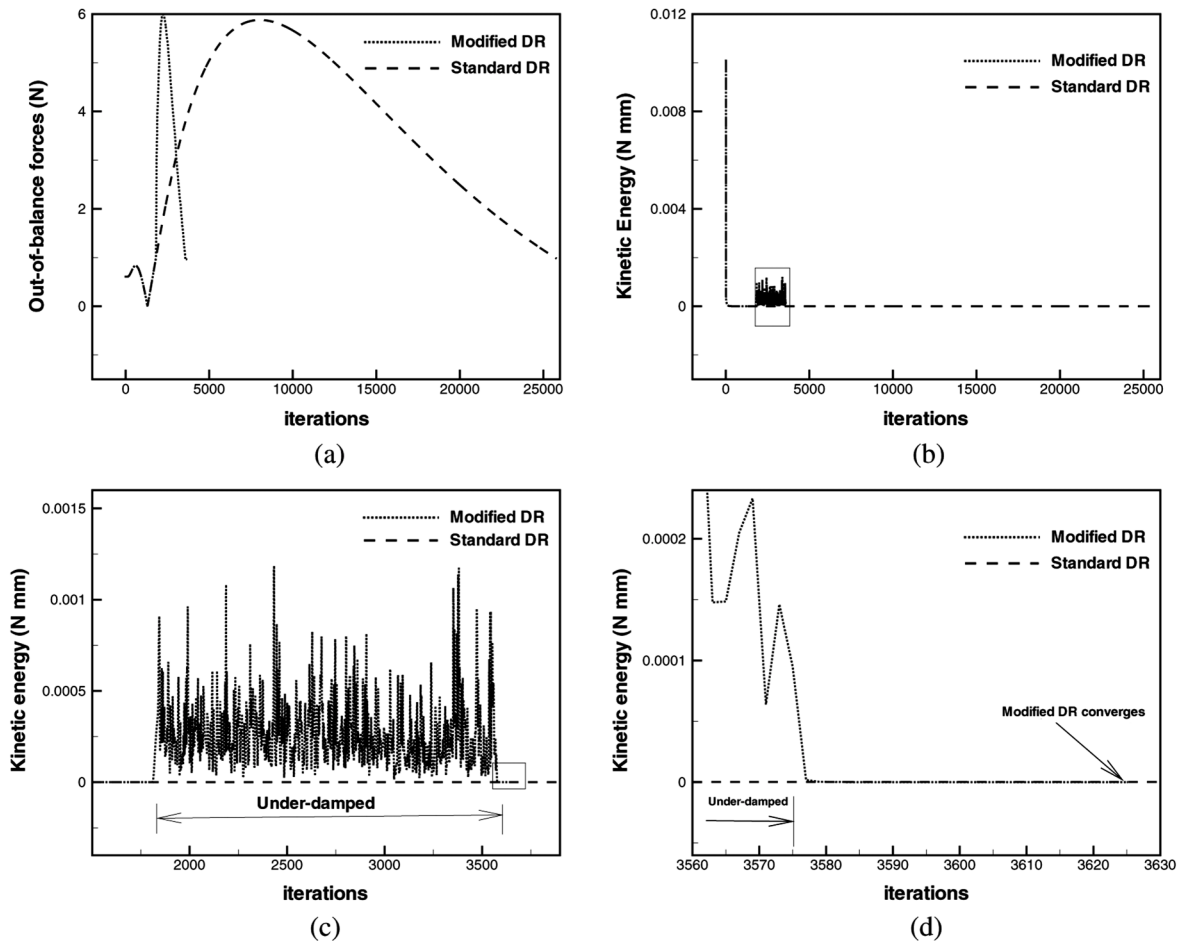


Fig. 4 Comparison between the standard and modified DR procedures: (a) Out-of-balance forces and (b) kinetic energy corresponding to the small specimen during the second phase in the step for an imposed displacement of $\delta = 0.0224$ mm. Successive zooms of the kinetic energy curve: (c) noisy response due to underdamping and (d) final achievement of convergence with critical damping.

standard DR method to converge, whereas the modified DR method only needs 3625. It is not possible for us to make a comparison in a situation of higher non-linear conditions—for instance a situation involving many cohesive elements and possible insertions at the same step— simply because the normal DR method would take too long to arrive at the solution of the static system.

The performance of the precautions taken to avoid overshooting can be evaluated by comparing the results given by both methods. For this purpose we have rendered the contour plots corresponding to the stresses along the x axis (σ_{11}) in Figs. 5a and b. Since the stresses are updated according to the converged solution, the stress distribution given by the standard and by the modified DR methods look so alike that it is not possible to differentiate between them. In passing we can notice that the crack does not propagate uniformly across the width of the beam but rather has a convex front.

We have also rendered the variable called “damage” in Fig. 6. It is defined as the fraction of the expended fracture energy over the total fracture energy per unit surface. Thus, a damage density of

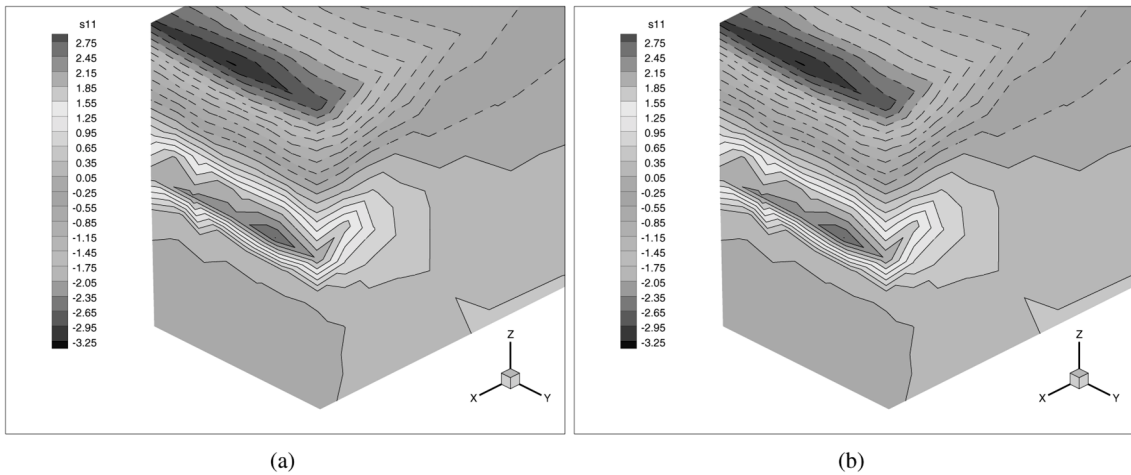


Fig. 5 Stress σ_{11} comparison at middle surface for (a) the normal and (b) the modified damping procedures for the small specimen ($D = 75$ mm) at an imposed displacement of 0.0224 mm. Dotted contour lines represent compressive stress values whereas solid contour lines stand for tensile stress values. The legend is in MPa.

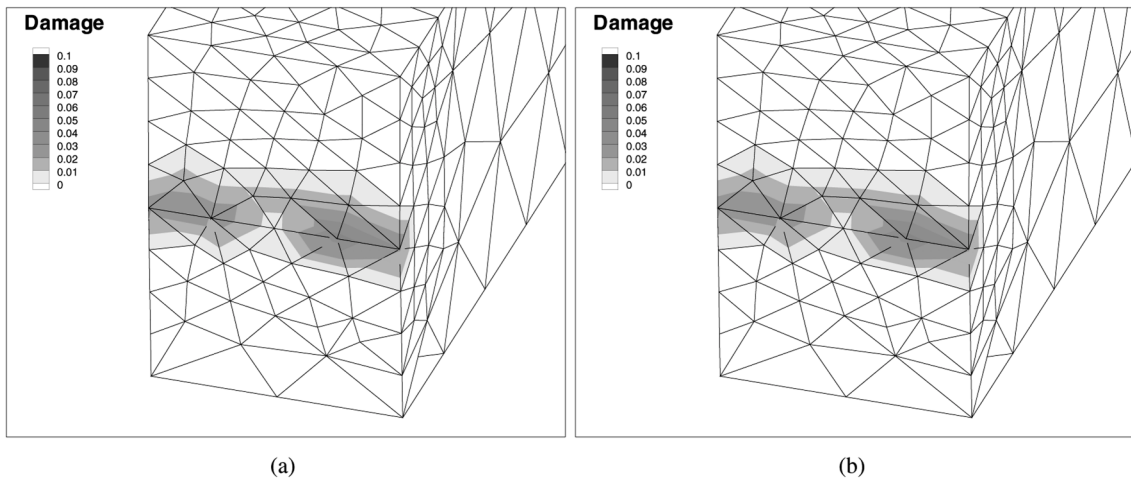


Fig. 6 Cohesive damage comparison at middle surface for (a) the normal and (b) the modified damping procedures for the small specimen ($D = 75$ mm) at an imposed displacement of 0.0224 mm.

zero denotes an uncracked surface, whereas a damage density of one is indicative of a fully cracked or free surface. As it stems from the definition, this variable is proper of cohesive elements only. Regrettably, our rendering tool reads the values of the variables at the nodes and interpolates them to get the contour plot (the values are actually computed at the Gauss points and interpolated to the nodes by the program). This is why in Fig. 6 the damage spreads out of the cohesive elements. In fact, only the elements where the damage is positive in all the nodes are cohesive: a careful observation of the figure allows recognition of the six elements present at the end of the step—the two elements inserted in the step only have a node in the notch tip—which confirms that the growth of the crack is not uniform. Regardless, it is not that difficult to observe that Figs. 6a and b

look alike. Again, the numerical differences in the damage incurred using the standard and the modified methods are very small and cannot be resolved in the contour plot.

All the aforementioned considered, we can conclude that both methodologies lead to the same results and that overshooting is avoided completely. Likewise, it is pertinent to reiterate here that the loading steps have to be kept small so that the cohesive elements are inserted gradually. Physically, this is consistent with a stable crack propagation. Otherwise, it would be the case of an unstable crack advancement for which neither the standard nor the modified DR method would find a corresponding static solution. We should have in mind that there may be cases in which static loading leads to unstable crack propagation, the so called “negative” geometries in Fracture Mechanics terminology, and again the DR method cannot handle them. In the end, the methodology that we propose here is close to the actual mechanics of crack propagation, which can be stable but are never absolutely static.

5.2. Validation against experimental results

5.2.1. Load-displacement curves

The load versus displacement curve for specimens of three different sizes, compared with the experimental results are shown in Fig. 7.

The model reproduces fairly well the P - δ response of the beams. The calculated maximum load only differs 0.4% from the experimental one for the small specimen, 3.0% for the intermediate one and 10.0% for the large specimen, which is specially remarkable if we have in mind that all the parameters feeding the model are measured experimentally and that we are using a standard cohesive law. Fig. 7 depicts two horizontal dashed lines to aid the direct visualization of size effect. The one at the level of 800 N indicates the load peak of the small beam, whereas the one which is above it marks the load level corresponding to twice such load. The load-peak of the intermediate

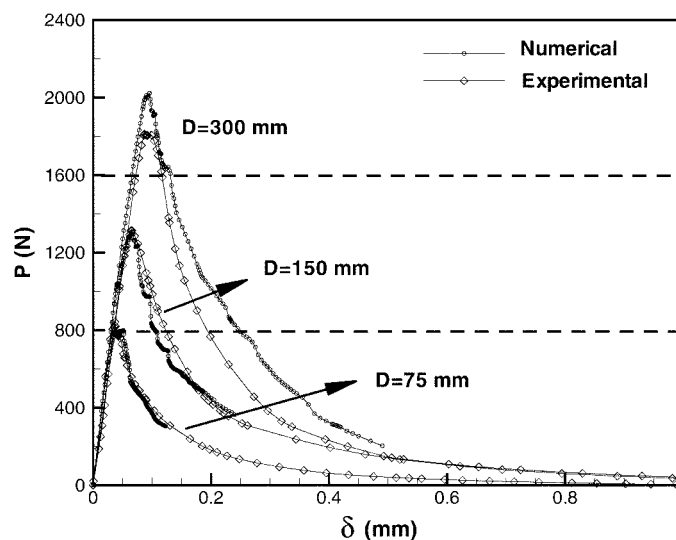


Fig. 7 Experimental and numerical load-displacement curves for specimens of three different sizes

beam does not reach that second line in spite that its size doubles the one of the small beam, indeed it only gets a 70% increase. Likewise, the load-peak given by the big beam is only 30% bigger than the one of the intermediate (the simulation gives a 50% increase). The experimentally observed size effect comes naturally from the simulations.

The post-peak behavior is also properly caught by the model. Particularly the simulations for the small and intermediate specimens give curves that are very close to the ones recorded in the experiments. The numerical softening branch corresponding to the big beam slightly deviates from its experimental counterpart, although such a difference can be registered between two identical actual beams due to the intrinsic concrete heterogeneity.

Nevertheless, the model is not that efficient when it comes to simulate the tail of the P - δ curves. On the one hand, the degree of fragmentation by the end of the test is very high. On the other hand, as the specimen is almost split, the displacement increase needed for variations in the loads and internal variables of the elements is high. Consequently, the number of iterations to achieve convergence increases dramatically at the end of the test and the run has to be stopped.

5.2.2. Fracture patterns

Three snapshots of the fracture patterns on mid-plane for each one of the simulated specimens are shown in Fig. 8, where the displacements have been magnified 100 times to aid visualization. Also shown in the figure are the level contours of damage, as defined above in 5.1. The transition zone wherein the damage variable takes intermediate values may be regarded as the cohesive zone, and the crack front may conventionally be identified with the level contour of 1/2. As it is normal in notched three-point bending tests, the real crack patterns were straight lines starting from the notch tip and ending in the loading point. Of course, such pattern is easily reproduced by the model. Indeed, our approach could be readily used in mixed-mode loading cases, which usually generate more complex fracture patterns than the case we are considering now.

Figs. 8a, d, and g correspond to the peak loads for the small, intermediate and big size beams respectively. The snapshots in Figs. 8c, f and i catch the moment where the beams are almost completely broken, while Figs. 8b, e and h represent a point in between which shows how the fracture zone has developed. For all the sizes it can be noticed that in the peak load the fracture zone has developed to some degree, but that the crack surfaces are not fully open yet. Later on, the same zone is more developed while new surfaces are open and the crack front propagates in a non-uniform way, which can only be observed in a full three-dimensional modeling. It is interesting to note that the crack front is convex in the direction of propagation, a feature which is characteristic of mode-I crack growth, the exterior of the crack front ostensibly lags behind the interior points. In Figs. 8c, f and i the crack continues to grow until the specimen is almost completely split and loses its strength.

6. Conclusions

We have put together a modified explicit dynamic relaxation method in conjunction with the cohesive theory to solve the static multi-cracking fracture process in a three-point-bend concrete beam. In calculations, the fracture surface is confined to inter-element boundary elements and, consequently, the structural cracks predicted by the analysis are necessarily rough. Even though, this

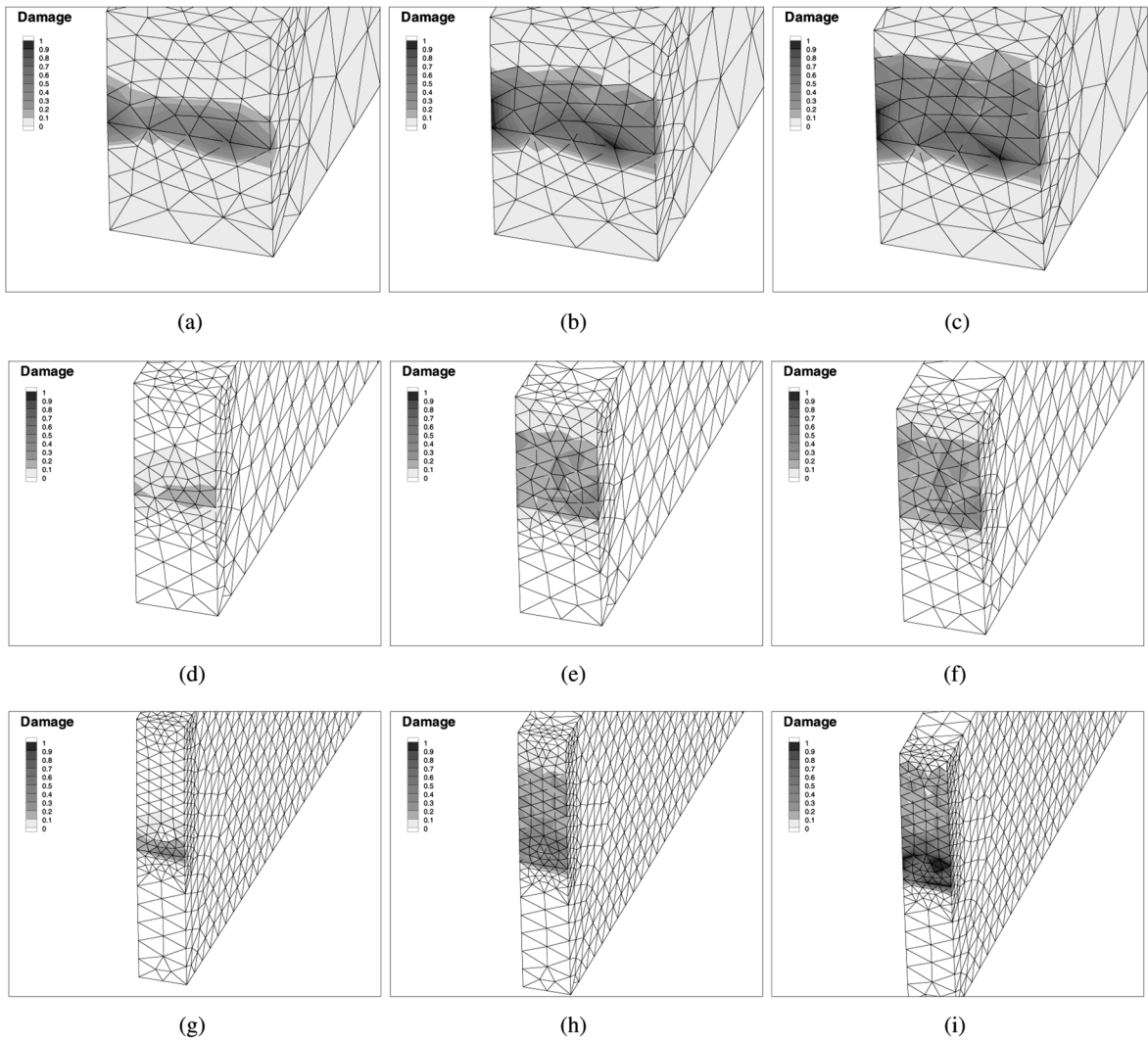


Fig. 8 Snapshots of the fracture patterns at middle surface developed at imposed displacements of (a) 0.05 mm, (b) 0.07 mm and (c) 0.11 mm respectively for the small specimen ($D = 75$ mm); (d) 0.074 mm, (e) 0.16 mm and (f) 0.24 mm for the middle size specimen ($D = 150$ mm); and (g) 0.1 mm, (h) 0.25 mm and (i) 0.50 mm for the large size specimen ($D = 300$ mm)

numerical roughness in concrete can be made to correspond to the physical roughness by choosing the element size comparable to the aggregate size, the thus-induced geometrical non-linearity and the material non-linearity inherent to concrete are hard to handle for traditional static solvers.

The explicit dynamic relaxation method, as an alternative, avoids the use of direct solvers as well as the large storage requirements associated with large matrices, making it specially attractive in computational mechanics (Sauvé and Metzger 1995). We have followed the ideas of Underwood (1983) and Oakley (1995b) for fictitious mass and damping matrices and implemented the explicit dynamic relaxation method with a concept that is distinct from the standard one. An initial damping coefficient estimated from the system is adopted to enhance the motion instead of critically damping it

from the beginning. A criterion that measures the balance between reaction forces from the supports and externally applied forces is used to control the iterations in this stage. While the global kinetic energy is chosen to control the balance of accuracy and efficiency of the solution for the static system.

Overshooting is avoided by a simple strategy consisting of dividing each step into two distinct phases. The first one takes the system to the equilibrium point without activating any of the irreversible mechanisms to reproduce concrete fracture. The second phase starts once equilibrium is achieved. Then the fragmentation routine inserts as many cohesive elements as necessary and searches for the new equilibrium point. The stresses, strains, damage limits etc. are only updated at the end of the iteration process. Of course, the load-displacement increments are taken small compared to the scale of the problem to avoid a big extent of fragmentation and subsequent fracture activity at each particular step.

Three sizes of concrete beams with different depth were modeled to validate against the experimental results of Ruiz (1999). The results show that the model captures the peak load accurately, the load-displacement curve follows closely the experimental results before and after the peak load. A comparison of the convergence rate between the standard and the modified DR method reveals the modified concept eliminates the stalling part of the traditional DR method and makes it a feasible and efficient solution technique for the problem considered.

Acknowledgements

Financial support from the DGICYT, Spain, under grant MAT2003-0843, and from Ministerio de Fomento, Spain, under grant BOE305/2003. Rena C. Yu thanks the Ministerio de Ciencia y Tecnología (MCYT), Spain, for the financial support given under the Ramón y Cajal Program.

References

- Bazant, Z. P. and Planas, J. (1998), *Fracture and Size Effect in Concrete and Other Quasibrittle Materials*, CRC Press, Boca Raton, Florida.
- Brew, J. and Brotton, D. M. (1971), "Non-linear structural analysis by dynamic relaxation", *Int. J. Num. Meth. Eng.*, **3**, 436-483.
- Camacho, G. T. and Ortiz, M. (1996), "Computational modelling of impact damage in brittle materials", *Int. J. Solids Structs.*, **33**(20-22), 2899-2938.
- Chen, B. K., Choi, S. K. and Thomson, P. F. (1989), "Analysis of plane strain rolling by the dynamic relaxation method", *Int. J. Mech. Sci.*, **31**(11/12), 839-851.
- Comite Euro-International du Beton (CEB) and the Federation Internationale de la Precont (FIP) (1993), *CEB-FIP Model Code 1990*, Thomas Telford Ltd, London, UK.
- Cook, R. D., Malkus, D. S. and Plesha, M. E. (1989), *Concepts and Applications of Finite Element Analysis, third edition*, John Wiley & Sons, Inc., New York.
- Day, A. (1965), "An introduction to dynamic relaxation", *The Engineer*, **219**, 218-221.
- De Andrés, A., Pérez, J. L. and Ortiz, M. (1999), "Elastoplastic finite-element analysis of three-dimensional fatigue crack growth in aluminum shafts subjected to axial loading", *Int. J. Solids Structs.*, **36**(15), 2231-2258.
- Metzger, D. (2003), "Adaptive damping for dynamic relaxation problems with non-monotonic spectral response", *Int. J. Num. Meth. Eng.*, **56**, 57-80.
- Metzger, D. R. and Sauvé, R. G. (1997), "The effect of discretization and boundary conditions on the convergence rate of the dynamic relaxation method", *Current Topics in the Design and Analysis of Pressure*

- Vessels and Piping, ASME PVP* **354**, 105-110.
- Oakley, D. R. and Knight, N. F. J. (1995a), "Adaptive dynamic relaxation algorithm for non-linear hyperelastic structures. Part I. formulation", *Comput. Meth. Appl. Mech. Eng.*, **126**, 67-89.
- Oakley, D. R. and Knight, N. F. J. (1995b), "Adaptive dynamic relaxation algorithm for non-linear hyperelastic structures. part ii. single processor implementation", *Comput. Meth. Appl. Mech. Eng.*, **126**, 91-109.
- Oakley, D. R. and Knight, N. F. J. (1995c), "Adaptive dynamic relaxation algorithm for non-linear hyperelastic structures. part iii. parallel implementation", *Comput. Meth. Appl. Mech. Eng.*, **126**, 111-129.
- Oakley, D. R. and Knight, N. F. J. (1996), "Non-linear structural response using adaptive dynamic relaxation on a massively parallel processor system", *Int. J. Num. Meth. Eng.*, **39**, 235-259.
- Ortiz, M. and Pandolfi, A. (1999), "Finite-deformation irreversible cohesive elements for three-dimensional crack-propagation analysis", *Int. J. Num. Meth. Eng.*, **44**, 1267-1282.
- Otter, J. (1965), "Computations for prestressed concrete reactor pressure vessels using dynamic relaxation", *Nucl. Struct. Eng.*, **1**, 61-75.
- Pandolfi, A., Krysl, P. and Ortiz, M. (1999), "Finite element simulation of ring expansion and fragmentation", *Int. J. Fract.*, **95**, 279-297.
- Pandolfi, A. and Ortiz, M. (1998), "Solid modeling aspects of three-dimensional fragmentation", *Eng. Comput.*, **14**(4), 287-308.
- Pandolfi, A. and Ortiz, M. (2002), "An efficient adaptive procedure for three-dimensional fragmentation simulations", *Eng. Comput.*, **18**(2), 148-159.
- Papadrakakis, M. (1981), "A method for automated evaluation of the dynamic relaxation parameters", *Comput. Meth. Appl. Mech. Eng.*, **25**, 35-48.
- Pica, A. and Hinton, E. (1980), "Transient and pseudo-transient analysis of mindlin plates", *Int. J. Num. Meth. Eng.*, **15**, 189-208.
- Rericha, P. (1986), "Optimum load time history for non-linear analysis using dynamic relaxation", *Int. J. Num. Meth. Eng.*, **23**, 2313-2324.
- Ruiz, G., Elices, M. and Planas, J. (1999), "Size effect and bond-slip dependence of lightly reinforced concrete beams", *Minimum Reinforcement in Concrete Beams, ESIS Publications* **24**, 67-98.
- Ruiz, G., Ortiz, M. and Pandolfi, A. (2000), "Three-dimensional finite-element simulation of the dynamic Brazilian tests on concrete cylinders", *Int. J. Num. Meth. Eng.*, **48**, 963-994.
- Ruiz, G., Pandolfi, A. and Ortiz, M. (2001), "Three-dimensional cohesive modeling of dynamic mixed-mode fracture", *Int. J. Num. Meth. Eng.*, **52**, 97-120.
- Sauvé, R. G. and Badie, N. (1993), "Nonlinear shell formulation for reactor fuel channel creep", *Design Analysis, Robust Methods and Stress Classification, ASME PVP* **265**, 269-275.
- Sauvé, R. G. and Metzger, D. (1995), "Advances in dynamic relaxation techniques for nonlinear finite element analysis", *Trans. ASME* **117**, 170-176.
- Sauvé, R. G. and Metzger, D. (1996), "A hybrid explicit solution technique for quasi-static transients", *Computer Technology: Applications and Methodology, ASME PVP* **326**, 151-157.
- Siddiquee, M., Tanaka, T. and Tatsouka, F. (1995), "Tracing the equilibrium path by dynamic relaxation in materially nonlinear finite element problems", *Int. J. Num. Anal. Meth. Geomech.*, **19**, 749-767.
- Thoutireddy, P., Molinari, J. F., Repetto, E. A. and Ortiz, M. (2002), "Tetrahedral composites finite elements", *Int. J. Num. Meth. Eng.*, **53**, 1337-1351.
- Underwood, P. (1983), "Dynamic relaxation", *Comput. Meth. Trans. Anal.*, **1**, 145-265.
- Yu, R. C., Pandolfi, A., Coker, D., Ortiz, M. and Rosakis, A. J. (2002), "Three-dimensional modeling of intersonic shear-crack growth in asymmetrically-loaded unidirectional composite plates", *Int. J. Solids Struct.*, **39**(25), 6135-6157.
- Yu, R. C., Ruiz, G. and Pandolfi, A. (2004), "Numerical investigation on the dynamic behavior of advanced ceramics", *Eng. Fract. Mech.*, **71**, 897-911.
- Zhang, L. G. and Yu, T. X. (1989), "Modified adaptive dynamic relaxation method and its application to elastic-plastic bending and wrinkling of circular plates", *Comput. Struct.*, **33**(2), 839-851.